

# Distributions for Higgs + jet at hadron colliders: MSSM vs SM

Oliver Brein<sup>1 a</sup> and Wolfgang Hollik<sup>2b</sup>

<sup>1</sup> Institute for Particle Physics Phenomenology, University of Durham, DH1 3LE, Durham, United Kingdom

<sup>2</sup> Max-Planck-Institut für Physik, Föhringer Ring 6, D-80805 München, Germany

**Abstract.** We present pseudorapidity and transverse momentum distributions for the cross section for the production of the lightest neutral Higgs boson in association with a high- $p_T$  hadronic jet, calculated in the framework of the minimal supersymmetric standard model. We discuss the theoretical predictions for the differential cross sections at the Large Hadron Collider and the Tevatron. In particular, we present the differences in the distributions compared to the Standard Model.

**PACS.** PACS-key describing text of that key – PACS-key describing text of that key

## 1 Higgs + Jet in the Standard Model

The production of SM Higgs bosons in hadron collisions at the LHC will proceed mainly via gluon fusion ( $gg \rightarrow H$ ). The detection of a SM Higgs boson with a mass below 130 GeV at the LHC is rather difficult because the predominant decay into a  $b\bar{b}$ -pair is swamped by the large QCD two-jet background [1]. Therefore, only through observation of the rare decay into two photons is the inclusive single Higgs boson production considered the best search channel in this mass range at the LHC.

Alternatively, and in order to fully explore the Higgs-detection capabilities of the LHC detectors, one can investigate more exclusive channels like e.g. Higgs production in association with a high- $p_T$  hadronic jet [2]. The main advantage of this channel is the richer kinematical structure of the events which allows for refined cuts increasing the signal-to-background ratio, obtained at the price of a lower signal rate compared to the inclusive channel (about 10% of the rate of the inclusive process). For the SM Higgs boson, simulations of this signal process and its background, considering the decay channels  $H \rightarrow \gamma\gamma$  [3, 4] and  $H \rightarrow \tau^+\tau^-$  [5], have shown promising results for the ATLAS detector. Also, very recently, promising simulation results for the Tevatron appeared involving this process in connection with the decay  $H \rightarrow W^+W^-$  [6].

The partonic processes at leading order contributing to the hadronic reaction  $pp \rightarrow H + \text{jet} + X$  (see Fig. 1) are gluon fusion ( $gg \rightarrow gH$ , 50–70 % of total rate), quark–gluon scattering ( $q(\bar{q})g \rightarrow q(\bar{q})H$ , 30–50 % of total rate) and quark–antiquark annihilation ( $q\bar{q} \rightarrow gH$ , rate small). The hadronic cross section

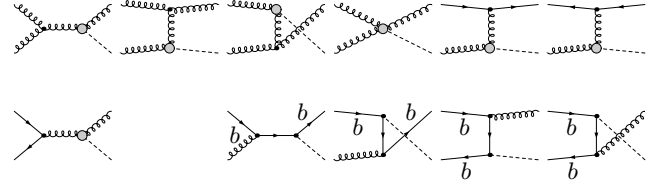


**Fig. 1.** Partonic processes contributing to  $pp \rightarrow H + \text{jet} + X$  in the SM. Hatched circles represent loops of heavy quarks. The depicted tree-level  $b$ -quark processes are much more important in the MSSM case.

is dominated by loop-induced processes, involving effective  $ggH$ - and  $ggHZ$ -couplings. If the  $b$ -quark is treated as a parton present in the proton, there are additional tree-level processes for quark-gluon scattering and quark-antiquark annihilation to consider. Yet in the SM, their contribution to the hadronic cross section is small.

A lot of progress has been made towards improving the SM predictions. The fully differential distribution for Higgs production at next-to-next-to-leading order QCD accuracy has become available [7], improved by resummation of logarithmically enhanced terms for low  $p_T$  [8]. Higher-order corrections to differential cross sections for a Higgs boson associated with a high- $p_T$  jet have been obtained explicitly: the next-to-leading order QCD corrections in the large top-mass limit [9] and, recently, the corresponding resummation of soft-gluon emission effects [10]. For the  $b$ -quark process  $bg \rightarrow Hb$ , the NLO QCD corrections are also known [11].

<sup>a</sup> Email: Oliver.Brein@durham.ac.uk (speaker)

<sup>b</sup> Email: hollik@mppmu.mpg.de

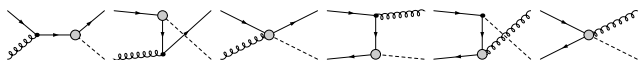


**Fig. 2.** Additional topologies for the loop-induced process  $gg \rightarrow qh^0$  and  $q\bar{q} \rightarrow gh^0$  in the MSSM. The hatched circles represent loops containing at least one gluino line.

## 2 Higgs + Jet in the MSSM

Motivated by the promising SM simulation [3, 4] we investigated the MSSM process  $pp \rightarrow h^0 + \text{jet} + X$ , involving the lightest MSSM Higgs boson [12]. Especially, as the process is essentially loop-induced, there are potentially large effects from virtual superpartners to be expected.

In the meantime, for this process,  $p_T$ -distributions have been studied in the limit of vanishing superpartner contributions at leading order [13] and were improved recently by soft-gluon resummation effects [14]. This limit is usually a good approximation when the superpartners are heavy, at a mass scale around 1 TeV. Quite recently, the SUSY-QCD corrections to the cross section and  $p_T$  distribution of the  $b$ -quark initiated processes  $bg \rightarrow h^0 b$  have been calculated [15].

In the MSSM, the classes of contributing partonic processes are basically the similar to the SM: gluon fusion  $g + g \rightarrow g + h^0$ , quark-gluon scattering  $q + g \rightarrow q + h^0$ , and quark-anti-quark annihilation  $q + \bar{q} \rightarrow g + h^0$ . While gluon fusion is an entirely loop-induced process, the other two classes also get contributions from tree-level  $b$ -quark initiated processes (see Fig. 1). Those Born-type processes are in general dominant for  $m_A \lesssim 120$  GeV, while for large values of  $m_A$  the loop-induced processes dominate. This behaviour is essentially a consequence of the Yukawa-coupling of the lightest MSSM Higgs boson to  $b$ -quarks, which can be enhanced for low values of the  $A$ -boson mass  $m_A$ . Formulae for the relevant couplings occurring in this process in our notation can be found in [12, 16].

The presence of superpartners in the loop contributions of the MSSM modifies the overall production rate for supersymmetric Higgs bosons compared to the production of SM Higgs bosons of equal mass. Moreover, there are new Feynman graph topologies containing at least one gluino line in the MSSM (see Fig. 2) which also affect the angular distributions and, at the level of hadronic processes, change rapidity and transverse-momentum distributions of the Higgs bosons or the jets, respectively.

## 3 MSSM results

In the following discussion we want to illustrate the MSSM predictions for the pseudorapidity,  $\eta_{\text{jet}}$ , and transverse momentum ( $p_T$ ) distributions of the hadronic processes  $pp \rightarrow h^0 + \text{jet} + X$  and  $p\bar{p} \rightarrow h^0 + \text{jet} + X$  and outline differences between MSSM and SM predictions. To compare a given MSSM scenario with the

SM, we choose the SM Higgs mass to have the same value as the  $h^0$  boson in that MSSM scenario. For the numerical evaluation, we use the cuts

$$p_T > 30 \text{ GeV}, \quad |\eta_3| < 4.5, \quad (1)$$

which have been used in previous Standard Model studies for the LHC [3, 4]. Details of the calculation and the MSSM parameter constraints taken into account can be found in [12, 17].

We show here results for the  $m_h^{\text{max}}(400)$  scenario, which is specified as follows.

The soft-breaking sfermion mass parameter is set to  $M_{\text{SUSY}} = 400$  GeV. The off-diagonal term  $X_t (= A_t - \mu \cot \beta)$  in the top-squark mass matrix is set to  $2M_{\text{SUSY}} (= 800 \text{ GeV})$ . The Higgsino and gaugino mass parameters have the settings  $\mu = -200$  GeV,  $M_1 = M_2 = 200$  GeV,  $M_{\tilde{g}} = 800$  GeV. When  $\tan \beta$  is changed,  $A_t$  is changed accordingly to ensure  $X_t = 2M_{\text{SUSY}}$ . The settings of the other soft-breaking scalar-quark Higgs couplings are  $A_b = A_t$  and  $A_f = 0$  ( $f = e, \mu, \tau, u, d, c, s$ ).

In the  $m_h^{\text{max}}(400)$  scenario, small values of  $m_A$  are still allowed. Hence we examine two Higgs sector scenarios:  $m_A = 110$  GeV,  $\tan \beta = 30$ , and  $m_A = 400$  GeV,  $\tan \beta = 30$ . The former leads to the dominance of  $b$ -quark initiated processes, while the latter is dominated by the loop-induced processes [12].

### 3.1 Differential cross sections at the LHC

The crucial parameter determining the properties of  $h^0 + \text{jet}$  production in the MSSM is  $m_A$  [12]. For  $m_A \lesssim 120$  GeV and  $\tan \beta$  not too small ( $\gtrsim 5$ ) the  $b$ -quark initiated processes dominate the production rate by far, while for larger  $m_A$  this role is taken over by the loop-induced processes. Accordingly, we split our discussion into the high- $m_A$  and low- $m_A$  cases.

#### 3.1.1 High $m_A$

The influence of rather light, yet not excluded, superpartners on the total hadronic cross section has been demonstrated to be strong [12]. In particular for the  $m_h^{\text{max}}(400)$  scenario with  $M_{\text{SUSY}} = 400$  GeV, the MSSM cross section for  $m_A > 200$  GeV and any  $\tan \beta \in [1, 50]$  is reduced by about 20 – 40% compared to the SM. Here, we investigate the impact on the shape of the differential distributions with respect to the SM.

The total hadronic cross section in the  $m_h^{\text{max}}(400)$  scenario is about 25% smaller than in the SM. Yet, as far as the  $\eta_{\text{jet}}$  and  $p_T$  dependent differences between MSSM and SM are concerned, the same qualitative picture appears. The variation of the relative difference  $\delta$  with  $\eta_{\text{jet}}$  in the range  $|\eta_{\text{jet}}| < 4.5$  is about 2% and with  $p_T$  in the range  $p_T \in [30 \text{ GeV}, 1000 \text{ GeV}]$  is about 7%.

The relative difference between the MSSM and SM prediction for the two-fold differential cross section  $d^2\sigma/dp_T/d\eta_{\text{jet}}$ , indicated by the contours in Fig. 4,

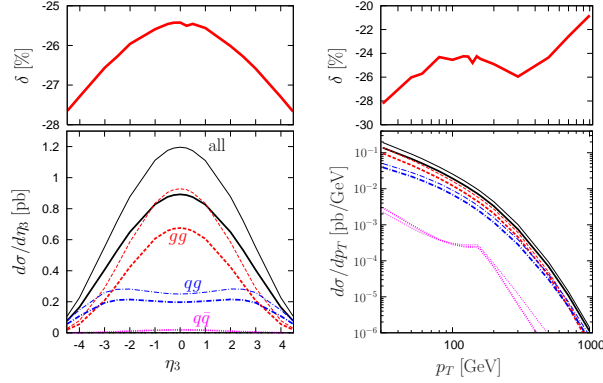


**Fig. 3.** LHC,  $m_h^{\max}(400)$  scenario with  $m_{A^0} = 400$  GeV,  $\tan\beta = 30$ : differential hadronic cross sections for Higgs + jet production and the relative difference,  $\delta$ , between the MSSM and SM prediction. Thick and thin lines correspond to the MSSM and SM prediction, respectively.

shows a non-trivial behaviour with an overall variation of more than 6% in the depicted range,  $|\eta_{\text{jet}}| < 4.5$  and  $30 \text{ GeV} < p_T < 500 \text{ GeV}$ . The differently shaped dots in Fig. 4 show the absolute difference between MSSM and SM, which gives an idea of the kinematical region where the LHC experiments may become sensitive to this difference.

Modifying the cuts may increase the sensitivity to deviations from the SM. Guided by Fig. 4, we study the cross section  $\sigma_f$  with rather soft forwardish jets and  $\sigma_c$  with harder more central jets:

$$\begin{aligned} \sigma_c &= \sigma(pp \rightarrow h^0 + j + X) \big|_{|\eta| < 1.5, p_T > 70 \text{ GeV}}, \\ \sigma_f &= \sigma(pp \rightarrow h^0 + j + X) \big|_{\substack{1.5 < |\eta| < 4.5, \\ 30 \text{ GeV} < p_T < 50 \text{ GeV}}}. \end{aligned}$$

Table 1 shows the results, where also the ratio

$$R = \frac{\sigma_c}{\sigma_f}, \quad (2)$$

and the relative difference between MSSM and SM

$$\Delta = \frac{R_{\text{MSSM}} - R_{\text{SM}}}{R_{\text{SM}}} \quad (3)$$

are listed. While each individual cross section in the MSSM and the SM is still of the order of 1 pb, which translates into  $10^5$  raw events for an integrated luminosity of  $100 \text{ fb}^{-1}$ , the MSSM ratio  $R_{\text{MSSM}}$  differs by 4.2% compared to  $R_{\text{SM}}$ .

### 3.1.2 Low $m_A$

As an example for the low- $m_A$  case at the LHC we show results for the  $m_h^{\max}(400)$  scenario in Fig. 5. The change with respect to the SM is dramatic. Due to the enhanced cross sections of the  $b$ -quark processes, the quark-gluon scattering contribution dominates the cross section and even the contribution from  $q\bar{q}$  is larger than from gluon fusion. The total hadronic cross section in the MSSM is 22 times higher than in the SM ( $\approx 175 \text{ pb}$ ).

quantity	SM	MSSM
$\sigma_c$	1.448 pb	1.096 pb
$\sigma_f$	1.419 pb	1.031 pb
$R = \sigma_c/\sigma_f$	1.020	1.063
$\Delta$		4.2%

**Table 1.** Cross section prediction in the  $m_h^{\max}(400)$  scenario for Higgs + jet production with jets radiated into the central ( $\sigma_c$ ) and forward part of the detector ( $\sigma_f$ ), together with their ratio  $R$  and the relative difference between the MSSM and SM value for  $R$ ,  $\Delta$ .

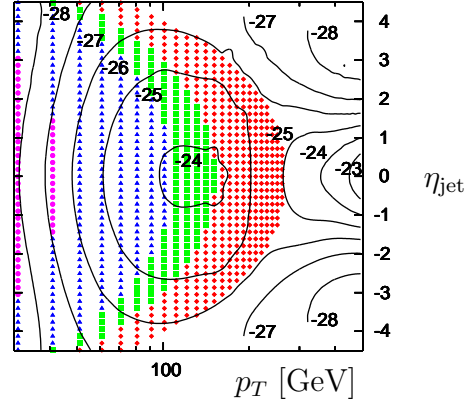


**Fig. 4.** Relative and absolute difference between the MSSM and SM prediction for  $d^2\sigma/d\eta_{\text{jet}}dp_T$  at the LHC for the  $m_h^{\max}(400)$  scenario with  $m_{A^0} = 400$  GeV,  $\tan\beta = 30$  as a function of  $p_T$  and  $\eta_{\text{jet}}$ . Contour lines show the relative difference in %, while diamonds ( $\blacklozenge$ ), squares ( $\blacksquare$ ), triangles ( $\blacktriangle$ ), circles ( $\bullet$ ), refer to an absolute difference in the range 0.1-0.5 fb/GeV, 0.5-1 fb/GeV, 1-5 fb/GeV, 5-10 fb/GeV respectively. In the white area the difference is less than 0.1 fb/GeV.

Out of all jets allowed by our cuts (1) a larger fraction of jets is radiated into the central part of the detector. For instance, the fraction of jets produced with  $|\eta_{\text{jet}}| < 2$  compared to all jets allowed by the cuts is 93% in the MSSM versus 85% in the SM. Correspondingly, the  $p_T$  spectrum is much softer than in the SM, yielding an enhanced rate for processes with jet transverse momenta below 850 GeV, e.g. by a factor of 10 for  $p_T = 100 \text{ GeV}$ , and rates similar to the SM above 850 GeV.

### 3.2 Differential cross sections at the Tevatron

The typical hadronic cross section for Higgs + jet in the SM expected at the Tevatron for the cuts  $p_T > 30 \text{ GeV}$  and  $|\eta_{\text{jet}}| < 4.5$  is around 0.1 pb for Higgs masses around 100 GeV, which is possibly not sufficient to be observable at the Tevatron. Therefore, for the Tevatron only the MSSM scenarios with low  $m_A$  and  $\tan\beta$  not too small are of interest. Those scenarios exhibit a cross section enhanced by a factor of up to 30 compared to the SM [12]. This is due to the contribution of  $b$ -quark initiated processes which become

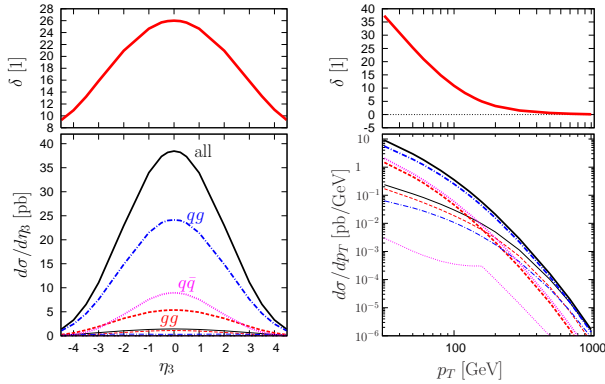


**Fig. 5.** LHC,  $m_h^{\max}(400)$  scenario with  $m_{A^0} = 110$  GeV,  $\tan \beta = 30$ . (See also caption of Fig. 3.)

dominant because of the strongly enhanced Yukawa coupling of  $b$ -quarks to the Higgs boson  $h^0$ .

Fig. 6 shows results for the same low- $m_A$  scenario as just described for the LHC in the previous paragraph. Very similar to the LHC case, we see a strongly enhanced total hadronic cross section with a softer  $p_T$  spectrum and a larger fraction of jets radiated into the central part of the detector than in the SM.

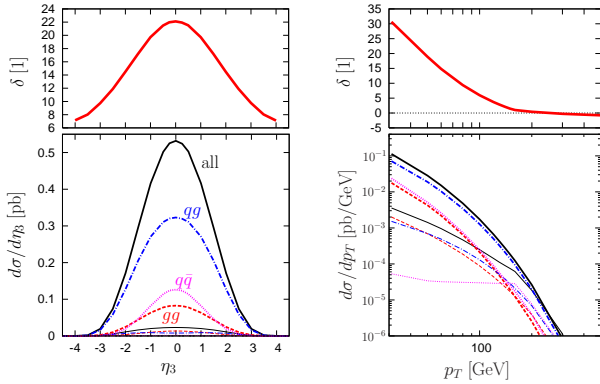


**Fig. 6.** Tevatron,  $m_h^{\max}(400)$  scenario with  $m_{A^0} = 110$  GeV,  $\tan \beta = 30$ . (See also caption of Fig. 3.)

## 4 Summary

We have calculated pseudorapidity and transverse momentum distributions for the MSSM  $h^0 + \text{high-}p_T$  jet production cross section at the LHC and the Tevatron. For scenarios with large  $m_A$ , the loop-induced processes dominate the cross section, and superpartners can have a significant impact when they are not too heavy. For small  $m_A$ , the Yukawa couplings of the  $b$ -quarks are enhanced and hence the cross section is dominated by  $b$ -quark induced tree-level parton reactions. The example investigated here, the  $m_h^{\max}(400)$  scenario, shows a strongly enhanced hadronic cross section compared to the SM, by a factor of more than 20. Such a scenario predicts for both LHC and Tevatron a softer  $p_T$  spectrum, with a fraction of jets radi-

ated into the central part of the detector larger than in the SM.

## References

1. CMS Physics Technical Design Report, Vol. II, CERN/LHCC 2006-021.
2. R. K. Ellis *et al.*, Nucl. Phys. B **297**, 221 (1988); U. Baur and E. W. Glover, Nucl. Phys. B **339**, 38 (1990); M. Chaichian *et al.*, Phys. Lett. B **198**, 416 (1987) [Erratum-ibid. B **205**, 595 (1987)].
3. S. Abdullin, M. Dubinin, V. Ilyin, D. Kovalenko, V. Savrin and N. Stepanov, Phys. Lett. B **431** (1998) 410.
4. V. V. Zmushko, ATL-PHYS-2002-020, IHEP-2002-23.
5. B. Mellado, W. Quayle and S. L. Wu, Phys. Lett. B **611** (2005) 60.
6. B. Mellado, W. Quayle and S. L. Wu, arXiv:0708.2507 [hep-ph], to appear in Phys. Rev. D.
7. C. Anastasiou, K. Melnikov and F. Petriello, Phys. Rev. Lett. **93** (2004) 262002, Nucl. Phys. B **724** (2005) 197.
8. G. Bozzi, S. Catani, D. de Florian and M. Grazzini, Phys. Lett. B **564** (2003) 65; S. Catani, D. de Florian, M. Grazzini and P. Nason, JHEP **0307** (2003) 028.
9. D. de Florian, M. Grazzini and Z. Kunszt, Phys. Rev. Lett. **82** (1999) 5209.
10. D. de Florian, A. Kulesza and W. Vogelsang, JHEP **0602** (2006) 047.
11. J. Campbell, R. K. Ellis, F. Maltoni and S. Willenbrock, Phys. Rev. D **67** (2003) 095002; S. Dawson, C. B. Jackson, L. Reina and D. Wackerroth, Phys. Rev. Lett. **94** (2005) 031802; S. Dittmaier, M. Kramer and M. Spira, Phys. Rev. D **70** (2004) 074010.
12. O. Brein and W. Hollik, Phys. Rev. D **68** (2003) 095006.
13. B. Field, S. Dawson and J. Smith, Phys. Rev. D **69** (2004) 074013.
14. U. Langenegger, M. Spira, A. Starodumov and P. Trueb, hep-ph/0604156.
15. S. Dawson and C. B. Jackson, arXiv:0709.4519 [hep-ph].
16. O. Brein and W. Hollik, Eur. Phys. J. C **13** (2000) 175; O. Brein, W. Hollik and S. Kanemura, Phys. Rev. D **63** (2001) 095001.
17. O. Brein and W. Hollik, Phys. Rev. D **76** (2007) 035002.